This article has been accepted for publication in a future issue of this journal, but has not been fully edited. Content may change prior to final publication. Citation information: DOI 10.1109/TSG.2020.2967937, IEEE Transactions on Smart Grid

Day-Ahead Market Participation of an Active Distribution Network Equipped with Small- Scale Compressed Air Energy Storage Systems

Mojtaba Jabbari Ghadi, Ali Azizivahed, Amin Rajabi, Sahand Ghavidel, Li Li, Jiangfeng Zhang, *Member*, *IEEE,* Miadreza Shafie-khah*, Senior Member, IEEE,* João P. S. Catalão*, Senior Member, IEEE*

***Abstract*— Large-scale compressed air energy storage (CAES) is conventionally used in power systems. However, application of CAESs at the distribution level is limited because of differences in design and efficiency. On the other hand, application of electrical batteries suited for distribution networks (DNs) faces also challenges from high investment cost and significant degradation. In this regard, this paper presents the participation of an active distribution system equipped with a small-scale CAES (SCAES) in the day-ahead wholesale market. To make CAES applicable to DNs, thermal-electrical setting design of the SCAES coupled with a packed-bed heat exchanger is adopted in the operation of the grid, where SCAES performs as an energy storage for DNs to surpass existing deficiencies of battery banks. The electrical/thermal conversion rate has been modeled for the SCAES operation. Moreover, the operation strategy of the SCAES is optimally coordinated with an electric vehicle charging station (EVCS) as an alternative energy storage technology in deregulated DNs. To make EVCS simulation more realistic, Gaussian Copula probability distribution function is used to model the behavior of the EVCS. The results obtained from different case studies confirm the value of SCAES as a reliable energy storage technology for DNs.**

***Index Terms*— Active distribution system, day-ahead wholesale market, small-scale compressed air energy storage, electric vehicles, solar distributed generation.**

M. Shafie-khah acknowledges the support by FLEXIMAR-project (Novel marketplace for energy flexibility), which has received funding from Business Finland Smart Energy Program, 2017-2021. J.P.S. Catalão acknowledges the support by FEDER funds through COMPETE 2020 and by Portuguese funds through FCT, under POCI-01-0145-FEDER-029803 (02/SAICT/2017). (*Corresponding authors: Miadreza Shafie-khah and João P. S. Catalão*).

M.J. Ghadi, A. Azizivahed, A. Rajabi, S. Ghavidel, L. Li, and J. Zhang are with the Faculty of Engineering and Information Technology, University of Technology Sydney, PO Box 123, Broadway, NSW 2007, Australia (Emails: {Mojtaba.JabbariGhadi,Ali.Azizivahed,Amin.Rajabi,Sahand.GhavidelJirsaraie}@student.uts.edu.au; {li.li,Jiangfeng.Zhang@uts.edu.au}.

M. Shafie-khah is with school of Technology and Innovations, University of Vaasa, 65200 Vaasa, Finland (e-mail: mshafiek@univaasa.fi).

J.P.S. Catalão is with INESC TEC and the Faculty of Engineering of the University of Porto, Porto 4200-465, Portugal (e-mail: catalao@fe.up.pt).

NOMENCLATURE

A. *Indices*

1) *Subscripts*

$1,2$	Index for inlet and outlet of SCAES compressor, PBHE, and expander
as	Index for air reservoir tank
f	Index for fluid
k	Index of PEV
par	Index for particle of heat exchanger
s	Index for solid
t	Index of time
$t1, t2$	Index for the time $t1$ and the time $t2$
vlm	Index for volumetric heat transfer coefficient

2) *Superscripts*

AE	Index for SCAES
al	Index for active power loss of the grid
ar	Index for arrival of PEVs to PEVs
B	Index for buses of the grid
buy	Index for buying power from day-ahead market
Com	Index for compressor
CS	Index for EVCS
cdf	Index for CDF based data generation
ch	Index for charging mode of SCAES
cm	Index for power consumption mode EVCS
D	Index for load demand
DA	Index for day-ahead market
di	Index for discharging mode of SCAES
dp	Index for arrival of PEVs to PEVs
EV	Index for PEV
Exp	Index for expanders
ex	Index for exported power to upstream grid
GR	Index for grid
ga	Index for exhausted gas
gm	Index for power generation mode of EVCS
im	Index for imported power from upstream grid
l	Index for branch number of grid
lo	Index for any pressure loss before air reaches the air store
PB	Index for PBHE
PV	Index for solar units
sel	Index for selling power to day-ahead market
tc	Index for hourly total capacity of EVCS

B. *Constants*

A	Area of heat exchanger
Bi	Biot number
$Ca^{(.)}$	Electrical capacity, $(.)=CHS/EV$
c_f	Specific heat capacity of the fluid mass

c_p Specific heat of the air in constant pressure
c^{PB} Specific heat capacity of PBHE
c_s Specific heat capacity of the solid mass
c_v Specific heat of the air in a constant volume
d_{par} Particle diameter
HR^{di} Fuel heat rate for discharging phase of SCAES
L_c Characteristic length scale for heat transfer
N_{Bus} Number of grid buses
N^{CS} Number of available chargers in EVCS
N_L Number of grid branches
N_T Number of hours in scheduling
NG Cost of natural gas
$\bar{P}_{NET}$ Maximum load demand of grid
$P_{max}^{AE,(.)}$ Maximum electric power of SCAES, $(.)=Com,Exp$
p_{Store}^{max} Maximum storage pressure in SCAES reservoir tank
R Specific molar gas constant
r The electrical resistance of branch
$S_{(.)}^{AE}$ Capacity of air tank of SCAES, $(.)=min,max$
$S_{(.)}^{AE}$ Air stored in SCAES tank $(.)=ini,Nt$ for first hour, last hour
$SOC_{(.)}^{EV}$ SOC of PEVs when entering EVCS, $(.)=min,max$
T_0 Temperature of ambient
$V_{min}^{AE,(.)}$ Minimum energy equal to compressed/expanded air $(.)=ch,di$
$V_{max}^{AE,(.)}$ Maximum energy equal with compressed/expanded air $(.)=ch,di$
$VOM^{(.)}$ Variable operating cost of SCAES, $(.)=ch,di$
γ Ratio of specific heats defined as c_p/c_v
γ^{CS} Charging/discharging capacity of chargers in EVCS
$\eta^{CS,(.)}$ Efficiency of chargers in EVCS, $(.)=cm,gm$
$\eta_{p,(.)}$ Polytropic efficiency, $(.)=ch,di$ for charging and discharging
Δm Each increment of air
Δz A slice of height in PBHE
ε Void fraction
$\pi^{(.)}$ Price of electricity in the day-ahead market, $(.)=sel,buy$

C. *Variables*

$a^{(.)}$ Energy conversion rate of SCAES, $(.)=ch,di$
B_d Exergy destruction in one of compressor, expanders, or PBHE
Bl Exergy remaining loss in one of PBHE, exhausted gas
E Level of electrical stored energy in EVCS
G Core mass velocity
h Enthalpy of the fluid
i Electrical current of branch
m Mass of air
n Number of potential serving-charger in EVCS
OC Operating cost of SCAES
P Electric active power
PC Operating cost of grid due to power loss
p Pressure of the fluid
Rev Revenue harvested from transactions with market
S Level of stored energy in air tank
SOC EVCS's state of charge
s Entropy of the fluid
T Temperature of the fluid
Tc Required time for charging PEVs
U Binary variable indicating ON/OFF or active/deactivate
V Energy equal with compressed/expanded air
Vol Per-unit of voltage at load points
v Velocity of the fluid
W Work
ρ Density of the mass
$\hat{h}$ Heat transfer coefficient
λ Thermal conductivity
η Energy efficiency of SCAES

I. Introduction

A. *Background and Scope*

Integration of distributed energy resources (DERs) into distribution level and utilization of various types of energy storage (ES) technologies and responsive loads have led to the emergence of new distribution grids which are known as active distribution systems (ADSs) [1]. The concept of ADS encompasses various aspects in which the capability of real-time monitoring of the network and the flexibility of DERs and ESs are of great importance to increase the hosting capacity of low-voltage grids. In recent years, there are extensive studies on ES technology and its applications in distribution grids [2, 3]. ES systems can help in creating a more resilient energy infrastructure and decreasing the costs of utilities and consumers. Compressed air energy storage (CAES) and electric vehicle charging station (EVCS) are two potential ES technologies to maximally exploit renewable energy resources since they can compensate the fluctuating nature of renewables. However, there are some uncertainties associated with EVCS due to inherent nature of plug-in electric vehicles (PEVs).

Based on the current technology, the investment cost for CAES system is much lower than other technologies like battery bank ES at the same capacities [2], while its lifetime is longer than battery banks. The utilization of CAES in ADSs can bring major benefits for the grid, and hence it is investigated in this paper.

In terms of cost, the capital cost for each kWh of a 2 MWh, 500 kW battery bank (Sodium Sulphur) is estimated at 1000–1400 $/kWh (total cost of $2–2.8 million [4]), while this cost for small-scale CAES (SCAES) is only around 360-650$/kWh (total cost of $0.72–1.3 million).

In terms of controllability, small-scale CAES can provide high ramp rates in several minutes. For the dynamic applications in microgrids which requires very fast responses within a minute, battery banks have some superiority over small-scale CAES, while for day-ahead scheduling which is operated hourly, capabilities of air turbines can assist small-scale CAES to provide suitable responses for power systems.

In terms of storage efficiency, the current efficiency of small-scale CAESs is not comparable with large battery banks. Roundtrip efficiency of battery banks exceeds 80%, while this parameter is about 70% for small-scale CAES with current technology. However, it should be mentioned that the technology of small-scale CAESs is not mature enough. As studied in [5], the technology progress of thermal storage unit and utilization of phase change materials can increase this efficiency to 85% during a short period of time.

The last points should be considered are in terms of the life cycle and operating costs. In both of these terms, small-scale CAESs have superiorities over the battery banks. Since no any chemical reactions involved, the life span of SCAEs can reach up to 25 years and also they only need limited operating and maintenance costs comparing to battery banks. Moreover, the number of charge/discharge operating cycles of small-scale CAEs is bigger than battery banks which shows the highly robust feature of small-scale CAES. Benefits of incorporating SCAES in ADSs are recommended in [6] to enhance the engineering

feasibility of the microgrids' participation in the day-ahead market.

Large-scale CAES systems (more than 3 MW and electric-to-electric efficiency of around 80%) have been studied for price arbitrage [7], supply-demand energy balancing and demand responses [8], to increase dispatchability, capacity factor, and total generation of wind power [9]. Besides, large-scale CAESs are employed for the participation in day-ahead energy markets [10], transmission capacity increase and transmission cost reduction [11], as a ES technology for energy hubs [12], and participation in the spinning reserve and reactive power markets [13]. The operation of large-scale CAES is also modeled; for example, Ref. [13] investigates the effects of thermodynamic models at the operating stages. In this regard, the thermodynamic effects of cavern SOC changes on the charging process, generation level on SOC, as well as discharging rate on heat rate are analyzed. This study also linearizes and adds some constraints obtained from the thermodynamics of each operation stage into electrical modeling of the CAES.

Besides the wide range of applications of large-scale CAES, this technology has a great potential to be used in smaller scales at the distribution level (0.3-3 MW) or micro-scales at residential communities (less than 0.3 MW). Recent literature has studied the thermal modeling of micro- and small-scale CAES (SCAESs) [4, 14-16]. Ref. [14] provides an experimental evaluation of a micro-CAES coupled with a wind turbine. The necessity for a resilient thermal storage unit is neglected in the thermal cycle modeling of [14], as the size of CAES is relatively small. In [15], the thermodynamic response of the charging and discharging cycles in the storage tank is numerically analyzed for a micro-CAES coupled with a solar system. Some predictions of the system parameters from the thermodynamic analysis are used as essential data for designing the tank, compressor, and expander. Authors in [16] present the experimental result of a pilot SCAES plant with a water tank as thermal storage. A detailed analysis of SCAES with packed beds as the thermal storage is investigated in [4], where a high efficiency packed bed heat-exchanger (PBHE) is proposed to reduce the waste of energy and the required volume of the tank.

Other studies have investigated the electrical utilization of SCAESs. Considering the small capacity of SCAESs, the most potential applications of SCAEs are in the case of microgrids and distribution networks (DNs). In this regard, an expansion planning is accomplished in [17] employing advantages of SCAEs coupled with wind power. The results demonstrate that the energy cost of the community and capacity of transmission lines are significantly reduced using the proposed configuration. Another joint operation of wind and SCAES for microgrid application is studied in [18]. A max-min operation approach has been considered to manage the uncertainty of wind power and minimize loss of the load and wind power curtailment. Similar objectives are considered in [19] to operate a microgrid including SCAES, wind, and micro dispatchable DGs to minimize operation cost of DG units as well as the penalty cost due to energy not supplied. Ref. [20] takes advantage of the high ramp rate and quick start-up time features of SCAES to mitigate fluctuations of renewable-energy in the mixed planning-operation programming of an islanded microgrid. Authors in [21] use SCAES for frequency control of a microgrid, where an airflow controller is designed for SCAES to control the power generation/consumption of the CAES system to maintain the frequency stable. An investigation on different configurations of joint SCAES and wind power for remote microgrids, as well as an overview of air and thermal storage for small/medium-scale CAESs, are provided in [22]. Besides, it presents a detailed operation investigation on the distributed hybrid application of diesel, wind, and SCAES for a specified microgrid. Authors in [23] implement a conceptual cost-benefit analysis for the presence of a SCAES at distribution level with a high penetration of DERs, based on load and renewable energy generation time-series of Saxony-Anhalt. In [24], maximum feeding time of diesel engine with CAES, the optimum volume of the tank, and minimum mass of the tank are investigated when a CAES is integrated with wind power. The application of SCAES at the DN using the same formulation of large-scale CAESs is presented in [25], where an expansion planning of microgrids is proposed to increase the capacity of existing networks using joint operation of SCAES and wind power. The objective of [25] is to minimize the total electricity payment to the grid as well as costs of equipment over the planning horizon.

Moreover, some other papers have studied the application of micro-CAESs in electrical systems. In this regard, a new modeling approach of micro-CAES as a demand response device in metropolitan areas is presented in [26]. Ref. [27] utilizes a micro-CAES as ES in a small-scale stand-alone photovoltaic (PV) power plant for a radio telecommunications base station. Optimal tank sizing of a micro-CAES combined with a PV system for residential buildings is studied in [28]. In [29], a model of non-supplementary fired CAES is presented in a hub of power and heat system. However, the electric-to-electric efficiency of ES units in [27] is only around 50% due to the lack of an efficient heat exchanger and also several simplifications to reach a linear model.

Another potential ES technology is to use the storage capacity of PEVs which has attracted significant attention of grid operators along with the fast involvement of PEVs in transportation systems, although charging/discharging procedures of PEVs have considerable impacts on DNs. The effects of large-scale PEVs in terms of environmental, economy, reliability, power losses, and voltage profile are discussed in [30-32]. In addition to distributed residential charging/discharging methodologies, finding a coordination method for EVCS as an integrated storage unit is a vital issue. Ref. [33] investigates this problem while considering power exchange limitations of the grid, and [34] considers further congestion management in a grid with renewable DERs. In [35], an optimization methodology for the operation modeling of an EVCS with the ability of battery swapping is presented. The developed day-ahead scheduling considers the uncertainty of batteries and electricity price using robust optimization. In [36], a convex model of EVCS scheduling is proposed to minimize the EV battery degrading cost and energy purchase cost from the upstream grid. Ref [37] proposes multiple charging options for EVCS to find the charging station with minimum charging cost, charging time, and traveling time. In [38], a new charging scheme for EVCS in a dynamic electricity pricing environment is developed which allows PEVs to share their stored energy with other vehicles under an aggregated framework.

B. Motivation, approach, and contributions

From the above literature review, there are a number of existing studies on the CAES applications in DNs. However, the thermal modeling of SCAES is a bit different from the large-scale CAES in the sense of efficiency, thermal modeling of heat exchanger unit, and loss destruction during compression and expansion procedures. Such differences have not been extensively noted in literature, and mostly existing studies still use the conversion rates of large-scale CAESs for small-scale ones, which will cause non-negligible inaccuracies. Indeed, the

This article has been accepted for publication in a future issue of this journal, but has not been fully edited. Content may change prior to final publication. Citation information: DOI 10.1109/TSG.2020.2967937, IEEE Transactions on Smart Grid

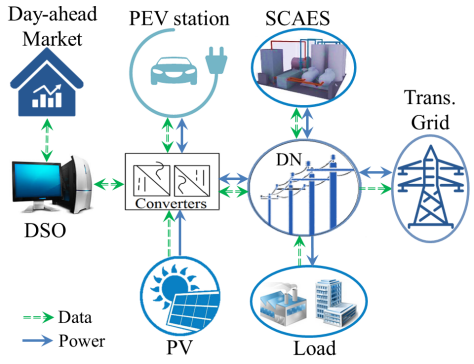

Fig. 1. Diagram illustration of proposed configurations

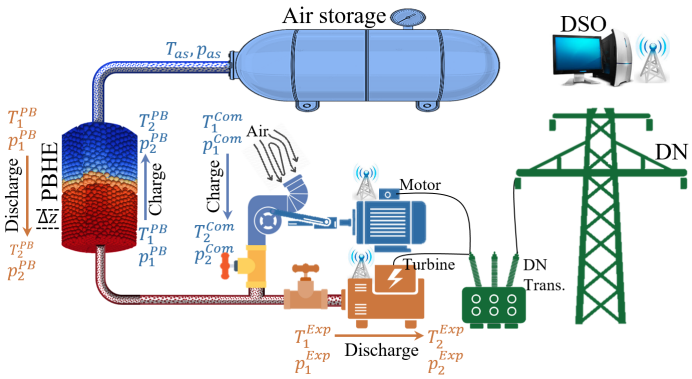

Fig. 2. A schematic of SCAES with packed bed heat exchanger

scale of an ES based on mechanical procedures has a significant impact on the total efficiency of the unit. Therefore, we develop a detailed SCAES model to cover both the thermal and electrical processes rather than simple electrical only formulations in literature. To simplify the thermal models, we also show that complex thermal formulations can be replaced by two new approximate thermal-to-electric and electric-to-thermal rates (i.e., different than large-scale CAESs) to make the models more convenient and less complicated for future applications. The modeling sections of SCAES in this study are based on practical results of implementing pilot SCAES. Additionally, the presence of thermal modeling of PBHE in the obtained models can make ES unit more efficient. In order to validate the model, the SCAES has been studied in a day-ahead scheduling case study.

Besides, there are also existing studies investigating the integration of EVCS in power grid operation, where the key issue in this case is the modeling technique of PEVs' charging/ discharging in relation to EVCS [39, 40]. Several techniques, as detailed in literature, are adopted in this respect to model electric load of the DN as the result of PEV charging. Note that it is important to reach an appropriate and realistic estimation for several key parameters like arrival time, departure time, and SOC of PEVs when entering EVCS. This study models all these parameters based on realistic data of a charging station, and Gaussian copula distribution function is also applied to determine the availability of PEVs' stored energy. Moreover, the effects and potential benefits from the join operation of SCAES and EVCS at the distribution level are also studied in this paper.

Therefore, in this study, a framework for the participation of a distribution system operator (DSO) equipped with a SCAES in the day-ahead market is proposed. Then a coordinated strategy for the joint operation of SCAES and EVCS is offered. DSO, as the owner of ADS, is responsible for the scheduling of PEVs and SCAES, and sells/buys energy from/to the market after getting power forecast from solar units to meet load demand and operating constraints. The proposed formulation considers the detailed electrical and thermodynamic models of SCAES, which can assist DSOs and distribution companies more accurately in grid operations.

Hence, the contributions of this paper are as follows:

- Developing a model of SCAES for DSO to participate in a day-ahead market, where SCAES is equipped with a PBHE so as to increase efficiency and reduce the size of on-land reservoir tank;
- Evaluating actual thermal-electrical conversion rate for SCAES at distribution levels based on thermal formulations and practical results;
- Modeling highly uncertain behaviors of PEVs in the form of EVCS using Gaussian copula distribution function, where EVCS is optimally coordinated with SCAES as an alternative energy storage;

The rest of paper is organized as follows. Section II discusses the structure of the proposed configuration as well as mathematic models of the energy market. Case studies and results for five scenarios with different schemes of RES/ESs participation are presented in Section III. Finally, Section IV draws a conclusion from the obtained results.

II. System Configuration and Mathematical Modeling

Fig. 1 shows the framework of the proposed configuration. As it can be seen, all the elements are individually controlled by DSO using a supervisory data-exchange system; while DSO is in contact with the transmission system operator to get data of day-ahead energy market. PV units as non-dispatchable distributed generation (DGs) provide power for DN through electrical converters. EVCS and SCAES are two different types of ES in the system with the ability to exchange power in both directions. While the power exchange of EVCS is accomplished by means of a bipolar converter, SCAES is directly connected to the grid. For an electric vehicle charging station, electric chargers are used to exchange power between the grid and EVs. Considering the fact that electric vehicle charging station is scheduled to receive power from EVs' DC battery during some hours and refill them during other hours, it necessitates employing a bipolar converter as the chargers. However, because of using the air turbine and an AC generator during the discharging periods of the small-scale CAES unit, it can be directly connected to the grid using a booster transformer. This configuration is designed to exploit sparks of energy price by charging and discharging of storage units during the scheduling horizon.

A. Formulation of small compressed air energy storage

Fig. 2 shows the schematic of SCAES. In order to avoid exergy loss during the charging mode, as it can be seen in this figure, a direct PBHE is located after the last compression stage (i.e., before the air enters into the tank), which reduces the required volume of storage [4, 16]. PBHEs are composed of solid particles with a high tolerance of temperature and pressure, which can provide high amounts of heat exchange while having relatively low-cost construction.

The value of different energy loss parameters during thermal operation of CAES is calculated through thermal modeling based on the air stored in the tank (i.e., obtained from the previous hour) and the required input/out power during charge/discharge. As an illustration, consider hour n is scheduled for compression based on the solution provided by the optimization algorithm. Then, considering the amount of air stored in the tank (i.e., a function of the status of CAES in previous hours) as well as the amount of power required to be stored for hour n, the value of thermal resistance and fluid pressure are different, which results in a specified fluid rate. In such the situation, the value of different energy losses during this mechanical procedure is calculated

This article has been accepted for publication in a future issue of this journal, but has not been fully edited. Content may change prior to final publication. Citation information: DOI 10.1109/TSG.2020.2967937, IEEE Transactions on Smart Grid

based on Section II-A-(1). Therefore, the compression rate is obtained which can be utilized in Section II-A-(2). A similar procedure is accomplished for an hour that is scheduled for expansion by using the thermal formulations presented in Section II-A-(1), to determine a^{di} which is used in Section II-A-(2)

1) Thermodynamic modeling of SCAES

In this section, a numerical model for an adiabatic SCAES with a direct PBHE is developed. Thermal formulations of the paper are mainly based on [4], while the value of CAES parameters in [23] as a practical implementation of SCAES are involved to propose valid design parameters for the presented SCAES. Compared with large-scale CAESs, the results of thermal simulations in this paper demonstrate new thermal-electrical rates in both phases of compression and expansion which are valid based on the experiment results offered by [23].

As such, an average actual value is obtained for thermal-electrical efficiency of SCAES (i.e., suitable for DNs operation). As opposed to studies which have inappropriately used the SCAES with the same design setting of the large-scale CAES, implementation of thermal formulations in this paper provides a key reference value for electrical modeling that omits necessity for running a thermal model in future studies.

a. Compression and expansion

Thermal modeling for compression and expansion modes of SCAES can be mathematically represented as follows. In this regard, the work and energy destruction in each mode are formulated. Then, actual electric-to-thermal and thermal-to-electric rates are calculated for applying to electrical modeling.

All works are estimated by the energy conservation law in volume control mode while neglecting variations in potential and kinetic energies from inlet to outlet [41].

$$\frac{\dot{W}^{\psi}}{\dot{m}^{\psi}} = c_p\left(T_2^{\psi} - T_1^{\psi}\right) \qquad \psi=Com, Exp \quad (1)$$

$$T_2^{\psi} = T_1^{\psi}\left(p_2^{\psi}/p_1^{\psi}\right)^{\varpi} \qquad \varpi = \begin{cases}(\gamma-1)/\gamma\,\eta_p & \psi=Com\\ \eta_p\,(\gamma-1)/\gamma, & \psi=Exp\end{cases} \quad (2)$$

$$W_{\Delta m}^{Com} = \Delta m\; c_p T_1^{Com}\left(\left(\frac{p_{as}(m+\Delta m)+p_{lo}}{p_1^{Com}}\right)^{\frac{\gamma-1}{\gamma\,\eta_{p,ch}}} - 1\right) \quad (3)$$

$$W_{\Delta m}^{Exp} = \Delta m\; c_p T_1^{Exp}\left(\left(\frac{p_2^{Exp}}{p_{as}(m-\Delta m) - p_{lo}}\right)^{\frac{\eta_{p,di}(\gamma-1)}{\gamma}} - 1\right) \quad (4)$$

$$\frac{\dot{B}_d^{\psi}}{\dot{m}^{\psi}} = T_0\left(c_p \ln\frac{T_2^{\psi}}{T_1^{\psi}} - R\ln\frac{p_2^{\psi}}{p_1^{\psi}}\right) \qquad \psi = Com, Exp \quad (5)$$

The work per unit of mass in compressor/expander can be simply defined by (1). In the aforementioned formulations, (T_1 and T_2) are considered as the (input and output) temperature of the fluid when passing a procedure. For example, in the case of compression mode, T_1 is the temperature of ambient air and T_2 is the temperature of the air flowing out of the compression stage. The output temperature T_2 of the gas fluid in the charging/ discharging modes is calculated in (2) as a function of compression/expansion ratio p_2/p_1. Noteworthy, the pressure p_2 increases in the charging mode, as the storage pressure increases to approach p_{as}^{max}. There are the same symmetric variations for the pressure p_1 in the expansion mode. Then, based on (1) and (2), the required work for the compression of Δm is defined in (3) by adding the work needed to compress Δm to the required work to overcome tank pressure (i.e., as the result of previous compressions). p_{lo} is any pressure loss introduced before the air reaches the high pressure air store (e.g., by the after-cooling heat exchanger). Similar work formulation is defined in (4) for the discharge mode which depends on the current required expansion and storage pressure at previous state. Besides, the exergy destruction in compressor and expander is calculated by (5).

b. Packed-beds heat exchanger

In the PBHE, there are two components including fluid and solid gravel particles (solid phase). This section formulates changes of temperature in each of them in an incremental slice of PBHE over time as follows:

$$m_f c_f \frac{dT_f}{dt} = -v_f A \rho_f c_f \frac{dT_f}{dz}\Delta z - \hat{h}_{vlm} A \Delta z\left(T_f - T_s\right) \quad (6)$$

$$m_f = \rho_f \varepsilon A \Delta z \quad (7)$$

$$\frac{d\rho_f}{dt} = \frac{d\left(\rho_f v_f\right)}{dz} \quad (8)$$

$$(1-\varepsilon)\rho_s c_s \frac{dT_s}{dt} = -A\frac{d}{dz}\left(\lambda_s \frac{dT_s}{dz}\right) - \hat{h}_{vlm}\left(T_s - T_f\right) \quad (9)$$

$$m_s = \rho_s (1-\varepsilon) A \Delta z \quad (10)$$

Based on the law of energy conservation, the energy rate balance of PBHE is given in (6) for the fluid in a slice at height Δz and an aria A. In fact, from net heat input as the result of fluid flow in PBHE ($-v_f A \rho_f c_f \frac{dT_f}{dz}\Delta z$), a part will be exchanged with the solid phase ($-\hat{h}_{vlm} A \Delta z\left(T_f - T_s\right)$) and the rest ($m_f c_f \frac{dT_f}{dt}$) will be consumed to change fluid temperature. The mass of fluid in the slice Δz is calculated by (7). Due to changes in fluid temperature and pressure over the operation time, fluid density ρ_f will change as modeled by (10). Noteworthy, only temperature change rate on Z direction is considered and change rate in X and Y directions are neglected to simplify equations.

Similarly, energy rate balance for the solid phase is defined by (9); where temperature change rate of the solid phase of the PBHE ($(1-\varepsilon)\rho_s c_s \frac{dT_s}{dt}$) is equal to the summation of the heat conduction through the solid phase in the Z-direction $\left(-A\frac{d}{dz}\left(\lambda_s \frac{dT_s}{dz}\right)\right)$ and heat exchange with the fluid ($-\hat{h}_{vlm}\left(T_s - T_f\right)$). The mass solid in the slice Δz is calculated by (10).

In this paper, all formulations related to heat conduction between particles of PBHE are neglected. In other words, the temperature of particles are considered to be the same). This assumption is correct when the Biot number *Bi* (i.e., is calculated in (12) as a measure of the ratio of resistance to heat transfer via conduction to the resistance of heat transfer via convection) is much lower than 1. Based on the empirical formula (11) presented in [41], the volumetric heat transfer coefficient $\hat{h}_{vlm}$ between the gravel and air is given.

$$\hat{h}_{vlm} = 700\left(G/d_{par}\right)^{0.76} \quad (11)$$

$$Bi = \frac{\hat{h}\, L_c}{\lambda_s} = \frac{\hat{h}_{vlm} d_{par}}{2\lambda_{par} a_{par}} \quad (12)$$

Then, considering gravel particle diameter of 10 mm leads to a Biot number around 0.01. Because Bi$\ll 1$, it can be assumed that it is seldom necessary to solve the conduction equation [41].

c. Input/output formulation of SCAES

With the aim of thermal modeling of SCAES, this subsection formulates the input/output powers and efficiency of storage based on exergy destruction approach as follows [4, 42]:

$$W^{ch} = W^{di} + B_d^{Com} + B_d^{Exp} + B_l^{ga} + B_l^{PB} + B_d^{PB} \quad (13)$$

This article has been accepted for publication in a future issue of this journal, but has not been fully edited. Content may change prior to final publication. Citation information: DOI 10.1109/TSG.2020.2967937, IEEE Transactions on Smart Grid

$$Bl^{PB} = mc^{PB}T_0\left(\frac{T_{t1}^{PB}}{T_0} - \frac{T_{t2}^{PB}}{T_0} - ln\frac{T_{t1}^{PB}}{T_{t2}^{PB}}\right) \quad (14)$$

$$\eta^{AE} = W^{di}/W^{ch} \quad (15)$$

Exergy dispatch in the SCAES is formulated in (13) in which W^{Com} and W^{Exp} in charging/discharging cycles are determined by (3) and (4). Exergy destructions in PBHE are calculated by (5) for both charging/discharging modes. While B_l^{ga} is exergy loss in the exhaust gas exiting the final expansion stage, the Bl^{PB} referrers to exergy loss in PBHE. Assuming a constant specific heat capacity c^{PB} for PBHE, the exergy loss B_l^{PB} when the temperature in PBHE decreases from temperature T_{t1}^{PB} in the time $t1$ to T_{t2}^{PB} in the time $t2$ is determined by (14). Pressure drop in the PBHE is formulated based on the Ergun equation [42]. B_d^{PB} is the exergy destroyed in the PBHE from pressure losses and lengthwise conduction of heat along the bed and accounts for the remainder of the charge work. Value of this parameter is approximately equal to $B_l^{ga}+B_l^{PB}$ based on [16]. Finally Eq. (15) can be used to evaluate electric-to-electric efficiency of SCAES. Then, the values of charging conversion rate $a^{ch} = 1 - \left(B_d^{Com} + B_l^{PB,ch} + B_d^{PB,ch}\right)/W^{ch}$ and discharging conversation rate $a^{di} = 1 - \left(B_d^{Exp} + B_l^{ga} + B_l^{PB,di} + B_d^{PB,di}\right)/W^{di}$ are calculated to be used in electrical modeling of SCAES. In fact, instead of considering a constant value for the thermal-electrical conversion rates ($a^{ch/di}$) of SCAES, the value of these parameters during each charging/discharging cycle is evaluated based on the thermal formulations within each iteration of the algorithm. Then, the obtained results are substituted in (17) and (18). Besides, considering the fact that SCAES hourly charging/discharging energy of the unit is limited to its nominal range of operation, thermal constraints related to parameters like pressure and temperature for the piping system, compression/expansion stages, and thermal storage are satisfied within the operation horizon. However, in the case of storage component, the volume of compressed air into it needs to be controlled to prevent high pressure and temperature inside the tank. This amount is constrained to the maximum capacity of the storage unit by (22) and (23). In fact, the thermal limitations and constraints related to thermodynamics of SCAES are transformed and presented in electrical formulations.

2) Electrical modeling of SCAES

$$OC^{AE} = \sum_{t=1}^{N_T} P_t^{AE,ch}\, VOM^{ch} + P_t^{AE,di}(HR^{di}NG + VOM^{di}) \quad (16)$$

Noteworthy, in the case of SCAESs, the operating cost is a small value compared with the other daily operating costs of the DN. Besides, as opposed to large-scale CAES which needs a reheat procedure during discharge phases, there is no need for burning fuel for SCAES since the loss of energy in the PBHE is negligible [4]. Therefore, the total operating cost of SCAES can be regarded as a negligible amount and neglected in this research.

$$V_t^{AE,ch} = a^{ch}P_t^{AE,ch} \quad \forall t \quad (17)$$

$$P_t^{AE,di} = a^{di}V_t^{AE,di} \quad \forall t \quad (18)$$

$$V_{min}^{AE,ch}U_t^{AE,ch} \le V_t^{AE,ch} \le V_{max}^{AE,ch}U_t^{AE,ch} \quad \forall t \quad (19)$$

$$V_{min}^{AE,di}U_t^{AE,di} \le V_t^{AE,di} \le V_{max}^{AE,di}U_t^{AE,di} \quad \forall t \quad (20)$$

$$U_t^{AE,ch} + U_t^{AE,di} \le 1 \quad \forall t \quad (21)$$

$$S_{t+1}^{AE} = S_t^{AE} + V_t^{AE,ch} - V_t^{AE,di} \quad \forall t \quad (22)$$

$$S_{min}^{AE} \le S_t^{AE} \le S_{max}^{AE} \quad \forall t \quad (23)$$

$$S_{ini}^{AE} = S_{N_T}^{AE} \quad (24)$$

It is considered the system operator can exploit all the available air stored in the reservoir tank during the scheduling period. In the operation procedure of the SCAES, ambient air is compressed into the tank during the injection cycle by consuming $P_t^{AE,ch}$ and using electrical-thermal efficiency factor a^{ch} based on (17). A similar procedure for discharge mode is defined in (18); while charging/discharging energies of SCAES are limited by (19) and (20), SOC for the storage unit is formulated by (21). As indicated in (22), SCAES has a specified capacity which limits the total charging/discharging energy amounts. Obviously, the SCAES can operate in one of the charging or discharging modes during each hour as formulated in (23) where the initial amount of energy S_{ini} should be equal to the amount of stored energy at the last hour of scheduling $S_{N_T}^{AE}$ based on (24).

B. Formulation of DSO participation in day-ahead market

$$max\,[Profit] = Rev^{GR} - PC^{al} - OC^{AE} \quad (25)$$

$$Rev^{GR} = \sum_{t=1}^{N_T} P_t^{GR,ex}\pi_t^{DA,sal} - P_t^{GR,im}\pi_t^{DA,buy} \quad (26)$$

$$PC^{al} = \sum_{t=1}^{N_T} P_t^{al}.\pi_t^{DA,buy} = \sum_{t=1}^{N_T}\sum_{l=1}^{N_L} r^l(i_t^l)^2\,\pi_t^{DA,buy} \quad (27)$$

$$P_t^{PV} + P_t^{GR,im} + P_t^{AE,di} + P_t^{CS,gm} = P_t^{GR,ex} + P_t^{AE,ch} + P_t^{CS,cm} + P_t^{D} + P_t^{al} \quad \forall t \quad (28)$$

DSO aims to maximize its day-ahead profit by (25) which is defined as the difference between DSO's revenue of transaction with the market (selling/buying based on (26)) and the total operating costs (i.e., power losses and SCAES operation cost). Cost of active power losses of the network is formulated by (27). Balance of supply and demand is formulated in (28); while the uncertainty of solar units is neglected in this study.

C. Formulation of EVCS

The EVCS is considered as an ES unit in this research and formulated as follows.

$$0 \le P_t^{CS,\Lambda} \le P_t^{CS,tc}U_t^{CS,\Lambda} \quad \forall t, \Lambda = gm, cm \quad (29)$$

$$U_t^{CS,gm} + U_t^{CS,cm} \le 1 \quad \forall t \quad (30)$$

$$P_t^{CS,tc} = \gamma^{CS}n_t^{CS} \quad \forall t \quad (31)$$

$$n_t^{CS} = \min\left(N^{CS}, N_t^{EV,cdf}\right) \quad \forall t \quad (32)$$

$$E_t^{CS} = E_{t-1}^{CS} + P_t^{CS,cm}\eta^{CS,cm} - P_t^{CS,gm}/\eta^{CS,gm} + E_t^{CS,ar} - E_t^{CS,dp} \quad \forall t \quad (33)$$

$$E_t^{CS,\Re} = \sum_{k=1}^{n_t^{CS}} E_{t,k}^{EV,\Re} \quad \forall t, \Re = Arr, Dep \quad (34)$$

$$E_t^{CS} \le Ca^{CS} \quad \forall t \quad (35)$$

$$SOC_{min}^{EV} \le SOC_t^{EV} \le SOC_{max}^{EV} \quad \forall t, \forall PEV \quad (36)$$

$$TC^{EV} = \frac{Cap^{EV}(1 - SOC_t^{EV})DoD^{EV}}{\eta^{CS,cm}\,P^{EV}} \quad \forall t, \forall PEV \quad (37)$$

Power generation/consumption of EVCS is limited to the total capacity of EVCS by (29) and (30) in each hour; while this hourly capacity is calculated by (31) using the chargers' capacity and the number of available PEVs (n_t^{CS}). Parameter n_t^{CS} in (32) is constrained by the number of chargers and the number of PEVs entering to the station, generated by CDF which will be detailed in Section II-E. The power level of EVCS as calculated by (33) is changing continuously as the result of power exchange with the grid as well as the arrival/departure of PEVs (34); while the positive variable of E_t^{CS} should be limited within its nominal capacity of charging (35). From the other side, the EVCS operator sets a minimum SOC level for PEVs entering to the station by

This article has been accepted for publication in a future issue of this journal, but has not been fully edited. Content may change prior to final publication. Citation information: DOI 10.1109/TSG.2020.2967937, IEEE Transactions on Smart Grid

(36) to reach a higher amount of available reserve energy during peak hours. SOC_t^{EV} for each PEV can be obtained from $((AER - d_t^{EV})/AER) \times 100\%$ using the travelled distance (d^{EV}) and all-electric range (AER) [43]. Besides, the required time for recharging of PEVs is formulated by (37) based on their SOC and electrical specifications of battery and charger.

D. Formulation of the distribution grid operational constraints

Management of the grid is subjected to operating constraints as illustrated by (38)-(41).

$$0 \le P_t^{GR,im} \le \left(\bar{P}_{NET} + P_{max}^{AE,Exp} + Ca^{CS}\right) U_t^{GR,im} \quad \forall t \quad (38)$$

$$0 \le P_t^{GR,ex} \le \left(P_{max}^{AE,Com} + Ca^{CS} + P_t^{PV}\right) U_t^{GR,ex} \quad \forall t \quad (39)$$

$$0 \le U_t^{GR,im} + U_t^{GR,ex} \le 1 \quad \forall t \quad (40)$$

$$0.95 \le Vol_t^B \le 1.05 \quad \forall t \quad (41)$$

The importing power of grid considering the marginal situation of $P_t^{PV}=0$ is constrained by the aggregation of load demand and the power required for charging ES units (38); while considering the marginal state $P_t^D=0$, the exporting power to the upstream grid is constrained by the power provided by DERs and storage units (39). In (38) and (39), $P_{max}^{AE,Exp}$ and $P_{max}^{AE,Com}$ refer to maximum power of SCAES expander and compressor, respectively. Given the small amount of power loss, it is not included in these two marginal situations. To maintain the voltage power quality, the acceptable range for the voltage of buses is limited to [0.95, 1.05] by (41). In order to consider the network constraints for day-ahead operation while determining hourly voltage profile Vol_t^B of the buses and branch current i_t^l for power loss calculation, a direct iterative distribution AC power flow based on Bus-Injection to Branch-Current (BIBC) matrix $[BIBC]$ and Branch-Current to Bus-Voltage (BCBV) matrix $[BCBV]$ (42)-(44) [44] is run for each hour of scheduling (i.e., for each candidate solution of optimization algorithm). All DG and storage units are modeled as PQ sources.

$$I_i^k = I_i^r\left(V_i^k\right) + jI_i^i\left(V_i^k\right) = \left(\frac{P_i + jQ_i}{V_i^k}\right)^* \quad (42)$$

$$[\Delta V^{k+1}] = [BCBV][BIBC][I^k] \quad (43)$$

$$[V^{k+1}] = [V^0] + [\Delta V^{k+1}] \quad (44)$$

where V_i^k and I_i^k are the bus voltage and equivalent current injection of bus i at the k-th iteration, respectively. I_i^r and I_i^i are the real and imaginary parts of the equivalent current injection of bus i at the k-th iteration, respectively. The $[BCBV]$ and $[BIBC]$ matrix are calculated as in [44].

E. Copula modeling

It is a challenging issue to generate random inputs while maintaining their inherent dependence when they are not distributed based on standard multivariate probability functions. Besides, limited types of dependence can be modeled by some of the currently available standard multivariate distributions. Moreover, using these distributions cannot guarantee to reach sensible and real results. In this paper, the Copula distribution function (CDF) is employed to model the behaviors of the PEVs. Compared to other estimation methods, CDF can interpolate multivariate-data nonlinearly. A Gaussian copula is a modeling option to present the dependence between variables. For a d-dimensional copula, the Gaussian copula is a distribution over the unit cube $[0,1]^d$. The copula of $(X_1, X_2, \dots X_d)$ is defined as the joint cumulative distribution function of $(U_1, U_2, \dots U_d)$:

$$C(u_1, u_2, \dots c_d) = \Pr[U_1 \le u_1, U_2 \le u_2, \dots U_d \le u_d] \quad (45)$$

In fact, all dependence information between components of $(X_1, X_2, \dots X_d)$ are modeled in copula C. For a given correlation matrix $\mathcal{R} \epsilon [-1,1]^{d \times d}$, the Gaussian copula with parameter matrix $\mathcal{R}$ can be written as:

$$c_{\mathcal{R}}^G = \frac{1}{\sqrt{\det \mathcal{R}}} exp\left(-\frac{1}{2}\begin{pmatrix}\Phi^{-1}(u_1)\\ :\\ \Phi^{-1}(u_d)\end{pmatrix}^T .(\mathcal{R}^{-1}\text{-}I)\begin{pmatrix}\Phi^{-1}(u_1)\\ :\\ \Phi^{-1}(u_d)\end{pmatrix}\right) \quad (46)$$

where Φ^{-1} is the inverse cumulative distribution function of a standard normal, and I is the identity matrix. Noteworthy, there exists the reverse procedure for this modeling process which can be used to generate pseudo-random samples from general classes of multivariate probability distributions, and it is possible to generate a sample $(U_1, U_2, \dots U_d)$ from the copula distribution. Therefore, the required sample can be constructed by:

$$(X_1, X_2, \dots X_d) = \left(F_1^{-1}(U_1), F_2^{-1}(U_2), \dots, F_d^{-1}(U_d)\right) \quad (47)$$

Since PEV variables (including traveled distance and entry time to EVCS) are statistically dependent, a dual CDF is generated based on the actual data of PEVs [45]. A Gaussian CDF with correlation factor [1, 0.77665; 0.7766, 1] is used to generate the data. To this end, data from 50 PEVs are based for the generation of 2000 units (i.e., the number of vehicles in the fleet of PEVs under contract with EVCS).

F. Solution algorithms

The presented problem is divided into two sections. The first part is the thermal formulation of the problem which is solved using a finite step method (FDM). FDM is a numerical method for solving differential equations by approximating them with difference equations (i.e., using finite differences to approximate the derivatives). In our paper, FDM becomes a very good approximation for the work required when using mass increments equal to or less than 10^{-2} kg. Hence a mass increment of 10^{-2} kg is used for the numerical model to guarantee the convergence of the solution.

The second part of the problem (electrical part) is solved by swarm robotics search & rescue (SRSR) optimization algorithm. This algorithm was proposed by one of the authors in 2017 based on the artificial intelligence of a swarm of robots which are utilized for a search & rescue mission [46], and it has been compared with a number of previously presented algorithms in terms of convergence quality and convergence speed. Reasonable superiority of SRSR algorithm compared to previous optimization algorithms had been demonstrated in [46]. For benchmark functions, the SRSR was applied on several standard benchmark functions and a practical electric power system problem in several real-size case studies (i.e., unit commitment for thermal units with up to 100 generating units which includes more than 4800 mixed-integer and continuous variables) in medium and large scales. It is noted that the dimension of the current problem is much lower than those of previously solved by SRSR. Besides, while the evolutionary algorithms may not be reliable for real-time cases due to their stochastic natures, for day-ahead problems which operator has enough time to run the algorithm with a larger number of initial solutions and iterations, it is expected the algorithm to reach very close to optimal solutions which can be suitably utilized in real applications.

In this research, the number of initial solutions, and the number of function evaluation (as the stop criterion) are considered to be 100, 15000 respectively. There exist four control parameters in the optimization algorithm including movement factor, Sigma factor, Sigma limit, and Mu factor; while the first three factors are automatically tuned and the last factor is set to 0.7. The program has been run for 20 times and the best result has been presented in the paper. The execution time of the program (joint

This article has been accepted for publication in a future issue of this journal, but has not been fully edited. Content may change prior to final publication. Citation information: DOI 10.1109/TSG.2020.2967937, IEEE Transactions on Smart Grid

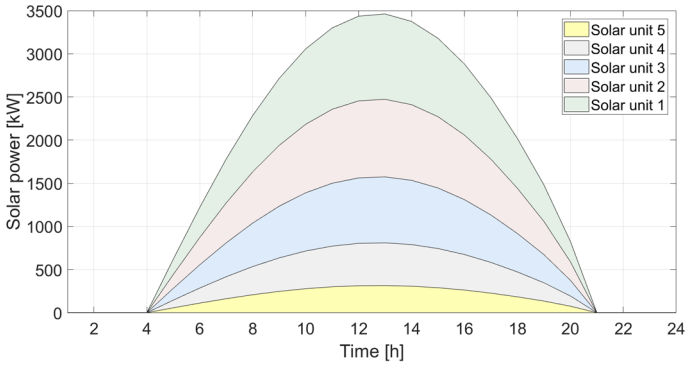

Fig. 3. Accumulative generation profile of solar DGs

thermal-electrical modeling) is about 7 minutes for each run. Since an evolutionary algorithm is employed for the optimization task, a constraint handling method based on penalty factors [47] is used to remove infeasible solutions which guarantees operational constraints are always met.

III. Case Study and Results

In this study, simultaneous cooperation of a SCAES and an EVCS as ES units is investigated for the participation of an ADS in the day-ahead energy market. IEEE 33-bus distribution network with the load-demands of 3.7MW and 2.3MVAR is used as the test system [48]. This research focuses on the daily operation of the ADS; therefore, previous studies are the basis to select the proper locations for the installation of solar DGs and ES units. The aim is to determine a daily operation of the DN to maximize the total profit of DSO (i.e., owner of the network's components) from participating in the market.

The production patterns of solar units (Fig. 3) located on buses 12, 17, 22, 31, and 33 are used for simulation [49]. The power factor of all PV units is considered 0.9 due to the presence of electronic converters. The detailed specification of adiabatic SCAES is provided in TABLE I.

The minimum capacity of SCAES corresponds to the pressure in which SCAES cannot provide a constant amount of power. Prices for sale/purchase of energy in the market are shown in TABLE II. Noticeably, the selling price is lower than the cost of electricity purchased from the grid due to transmission costs.

There are several types of PEVs (e.g. PEV-20, PEV-30, PEV-40, and PEV-60) based on AER factor in which the numeric index indicates the vehicle AER in terms of miles [43].

We use the PEV-20 in this paper that has proven its market potential over time. All cars in the fleet of PEVs have been considered to be manufactured by Nissan with a capacity of 100 kW and also have similar contracts with EVCS [50]. Based on a bilateral contract, EVCS operator uses PEVs with SOC not less than 50% when entering a parking station and the minimum duration of staying in the EVCS is 6 hours. In exchange for that, there is no parking cost for these vehicles. If a vehicle tends to leave the car park before this period, the car owner should pay a very low price of energy for the remaining hours. Transactions of other vehicles with EVCS are not modeled in this study. In the following, the conditions and assumptions for five scenarios are presented to validate the effectiveness of the proposed methodology. Then, the detailed investigation and comparison of the obtained results of different scenarios are provided in the last subsection.

TABLE I
Data for SCAES [4]

Max & Min capacity [kWh]	Motor capacity [kWh]	Generator capacity [kWh]	Location bus	Initial state [kWh]	Reservoir capacity [m^3]
2000 & 350	500	500	28	1000	182

TABLE II
Selling/Purchasing Energy Prices in Market [Cent]

Hour	1	2	3	4	5	6	7	8	9	10	11	12
Selling	63	53	51	50	51	52	63	67	73	80	80	80
Buying	106	106	106	106	106	106	106	125	135	135	135	135
Hour	13	14	15	16	17	18	19	20	21	22	23	24
Selling	70	69	73	79	80	71	66	67	72	77	67	63
Buying	135	135	135	135	135	135	135	125	125	125	125	106

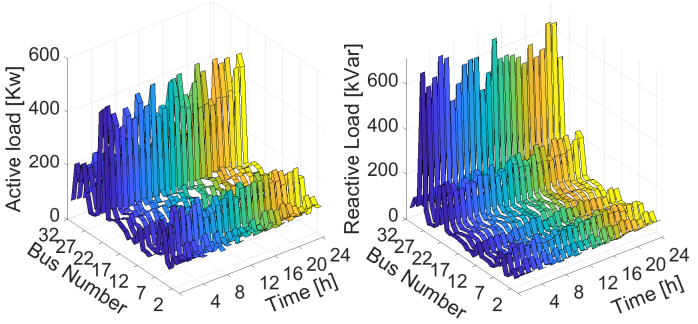

Fig. 4. Hourly active and reactive loads (24 hours) for 33-bus Network

1) Scenario 1: Base case

In this scenario, solar and ES units (EVCS and SCAES) are not considered in the model. This scenario provides base values for normal operation of the standard IEEE 33-bus DN.

2) Scenario 2: Without ES units

This scenario considers the presence of solar DGs while EVCS and SCAES are not involved in the grid operation. Voltage limit [0.95, 1.05] p.u. for buses is not applied in this case. Hourly loads of buses are generated using the normal distribution function that ranges within ±20% of the nominal load for all the scenarios. Active and reactive loads for network buses are shown in Fig. 4.

3) Scenario 3: Solar units and EVCS

This scenario investigates the simultaneous cooperation of PV units as generation sources and EVCS as ES unit. EVCS considers DOD as 0.4 to extend the life cycle of batteries. If SOC of a PEV at the leaving time is less than its initial charge level when entering the charging station, EVCS must pay the cost of the used energy at the price of the wholesale market. The EVCS uses level 3 chargers with a maximum capacity of 96 kW. The SOC and entrance time of PEVs using CDF are depicted in Fig. 5. It can be seen that the middle hours of the day have the highest power availability for EVCS.

4) Scenario 4: Solar units and SCAES

In Scenario 4, the EVCS unit in Scenario 3 is replaced by a SCAES system. Besides the electrical specifications detailed in TABLE I, the thermal constant factors of SCAES and PBHE are simulated based on the experiment results of [16] as well as the simulations of [4]. Two compression stages ($p_2 = 8.106\ Mpa$) are considered for SCAES while a pressure drop of 5 kpa is assumed for each packed bed which results in the pressure ratio

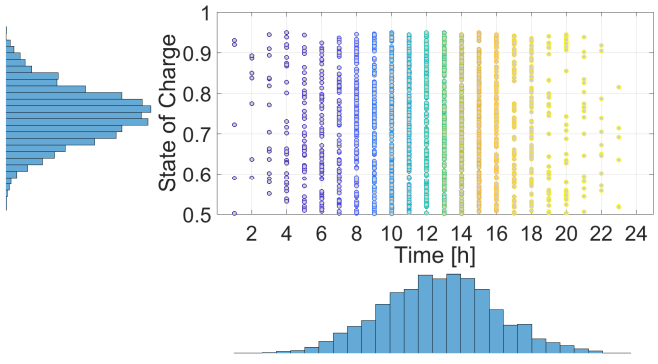

Fig. 5. PEVs' SOC and arrival time (EVCS located on bus 18)

This article has been accepted for publication in a future issue of this journal, but has not been fully edited. Content may change prior to final publication. Citation information: DOI 10.1109/TSG.2020.2967937, IEEE Transactions on Smart Grid

of $r = 8.97$). The minimum and maximum storage pressure are 2.027 and 8.106 MPa, respectively.

5) Scenario 5: Solar units, EVCS and SCAES

This scenario explores the benefit of simultaneously utilizing EVCS and SCAES. The potential advantages and weaknesses of each type of storage units are investigated in this scenario. The specifications of both ES systems are considered as same as the previous scenarios.

6) Comparison of results and discussions

In case of Scenario 1, the simulation result indicates that the hourly active loss of grid is 210.98 kW; while the voltage profile at bus 18 has the lowest value which is not within the acceptable voltage range 0.95~1.05 p.u. for the normal network operation. Since there is no generation unit, all the power needed to meet the demand should be purchased from the upstream grid.

However, as it can be deduced from Fig. 6, adding PV units in Scenario 2 cannot prevent bus voltage violation during certain hours of the day; as the sunlight is only available in the day time. Maximizing the net profit of daily operation of the grid is the ultimate aim of the DSO in a restructured power market. However, the operation conditions of the network play key roles in maintaining the security of operation as well as satisfying the quality of service. In this regard, changes of hourly active power losses and voltage profiles of buses, as two major operation factors, are illustrated in Fig. 8 and Fig. 7 for all the scenarios.

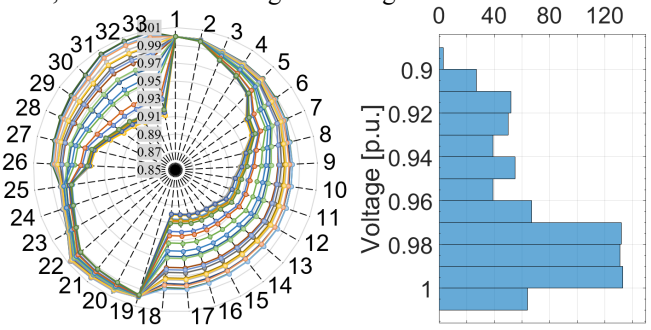

Fig. 6. 24-hour voltage profile of buses and relevant histogram; Scenario 2

Compared to the base case in which the changes of power loss solely follows the hourly variations of load demand, the power provision of solar DERs significantly reduces the power loss of the system. However, the amount of power loss in Scenario 2 is still not controllable since the solar units are not dispatchable. Surprisingly, the total/hourly power loss in most of the hours is increased by using only EVCS and SCAES in Scenarios 3 and 4, respectively; which is due to the profit maximization objective.

The availability of EVs in Scenario 3 and the charging pattern of SCAES in Scenario 4 are other reasons for such degradation. It can be seen that the simultaneous use of these two devices

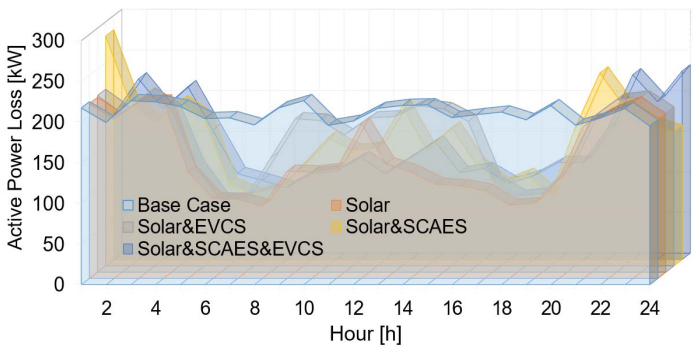

Fig. 8. Daily active power loss comparison of the grid, all scenarios

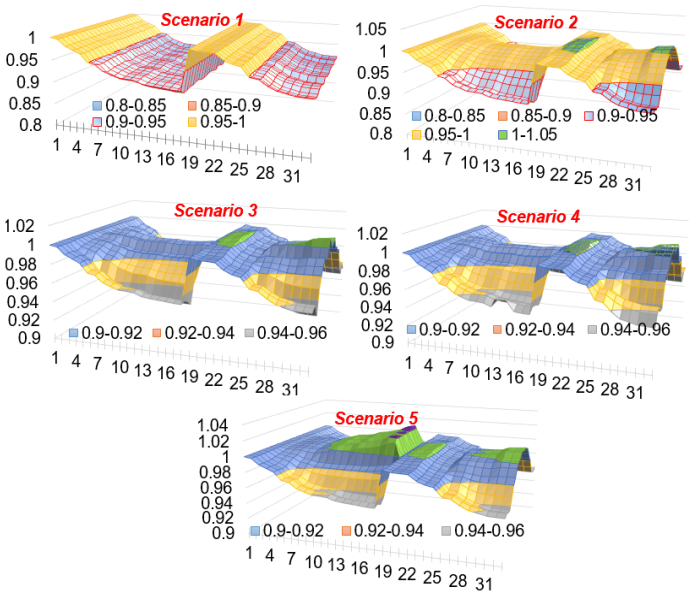

Fig. 7. Voltage profile of grid buses for 24h scheduling, all scenarios

provides a significant power loss reduction in Scenario 5. The energy provided during high accessibility of EVCS is exchanged with SCAES to control the power loss, which has a negative impact on the revenue of DSO. Noteworthy, certain availability of SCAES is a reason for the superiority of SCAES over EVCS.

In the case of the voltage profile of the network in Scenarios 1 and 2, the lack of generation causes the voltage violations at some buses of the grid in some hours. The other scenarios can sufficiently improve the voltage of buses to reach the defined range (0.95-1.05 p.u.). Despite similar voltage profiles in Scenarios 3 and 4, the indicator of voltage profile overall buses $\left(\sum_t^{N_T}\sum_B^{N_{Bus}}(Vol_t^B-1)^2/N_T.N_{Bus}\right)^{0.5}$ or these scenarios are 0.0224 and 0.0227 p.u., respectively which shows slight superiority of SCAES in terms of voltage improvement. This value for Scenario 5 is 0.0207 p.u. It is evident from Fig. 7 that employing both the EVCS and SCAES at the same time can considerably enhance the voltage profile to about 1.04 p.u. at some hours. Evidently, the voltage values at deep voltage points of the grid are set to near the lower margin of 0.95 p.u. for several hours, which means the algorithm does intend to sacrifice the profit for voltage profile enhancement.

Based on Fig. 9, the comparison of power provision and demand of EVCS in Scenarios 3 and 5 illustrates that the share of charging station generation is decreased after SCAES participation in Scenario 5. It can be inferred that no more generation is needed to reach the maximum profit despite having available capacity. The reason for not exploiting the full capacity of EVCS is that a large number of PEVs do not have SOC more than 50%. Moreover, scheduling should be accomplished in such

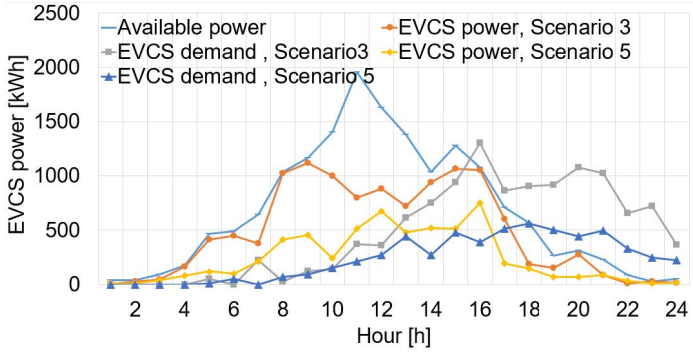

Fig. 9. Power provision and power shift of EVCS for 3rd and 5th scenarios

This article has been accepted for publication in a future issue of this journal, but has not been fully edited. Content may change prior to final publication. Citation information: DOI 10.1109/TSG.2020.2967937, IEEE Transactions on Smart Grid

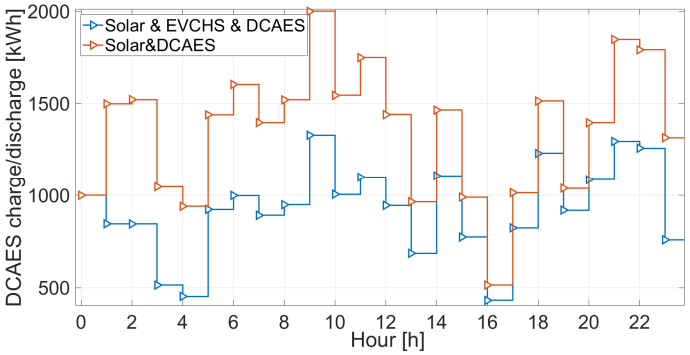

Fig. 10. Charge/discharge pattern of SCAES

TABLE III
FINAL COMPARISON OF DIFFERENT SCENARIOS

	Scenario 1	Scenario 2	Scenario 3	Scenario 4	Scenario 5
24h power loss [kW]	5055.9	3504.3	4037.3	3774.2	3434.7
Operation profit [$]	-11598.3	-6248.4	-5859.3	-5340.9	-4587.1

a way that energy received from PEVs returns to vehicles during the next hours. EVCS should adopt a demand management approach to control the usage of available batteries. In addition, a load shifting can be observed in both scenarios from peak demand hours of the main grid to the last hours of the day; this is due to the departure pattern of PEVs as well as optimization preference of the algorithm. The charging/discharging pattern of SCAES for Scenarios 4 and 5 is shown in Fig. 10. Similar to the EVCSs, the share of energy provision of SCAES is decreased in the joint operation, which means the coupled SCAES and EVCS can handle larger grids. Considering the load shifting of EVCS during the last hours of the day, which plays the role of extra demand, the SCAES can provide energy during these hours to maintain the security of the grid. Compared with the sole operations of ES systems in Scenarios 3 and 4, SCAES exploits nearly the full available capacity on hours 11 and 23 and provides $519 more profit in Scenario 4 considering the lower thermal-electrical conversion rate. Although EVCS is a dispatchable ES, some involving factors like availability of PEVs, maximum DOD, and minimum period of staying in EVCSs are critical factors, which downgrade the ultimate quality of EVCS services. Besides, SCAES can provide a uniform amount of at least 500 kW during the scheduling horizon; however, EVCS available capacity changes to much more/fewer amounts in some hours. A comparison of the daily power loss and DSO profit for five given scenarios is detailed in TABLE III; while the hourly transactions of DSO with the market are illustrated Fig. 11.

It can be seen that ES units aim to gain their profits from those hours, while PV units generate at their maximum power. This is

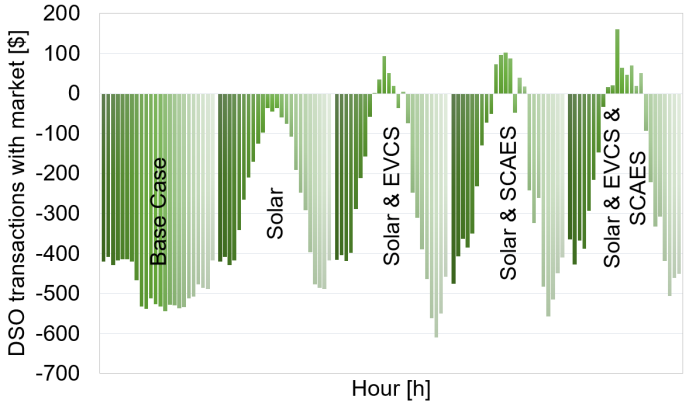

Fig. 11. 24h financial transactions of DSO with market

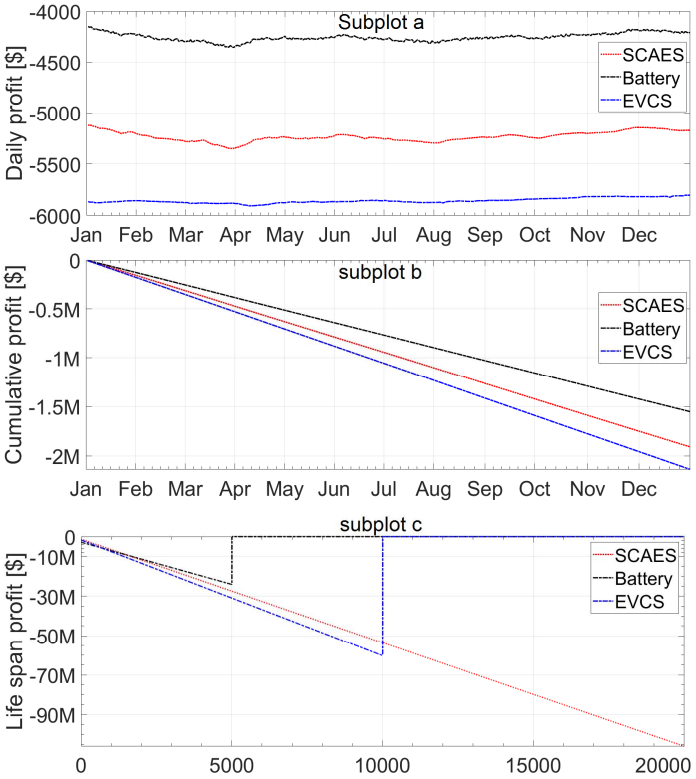

Fig. 12. Comparison of SCAES, Battery, and EVCS (a) daily DSO profit for a one-year period, (b) cumulative DSO profit for a one-year period, (c) cumulative DSO profit for the life span

because a large share of the total hourly load demand is met by the local generation, in particular for the hours when the energy price is high. Obviously, SCAES can reach a better performance compared to EVCS in terms of voltage profile, power loss, and profit maximization. This is mainly because of the uncertainties in PEVs' arrival and departure times and their SOC when arriving at EVCS. It should be noted that, this paper models the SCAES using practical thermal-electrical conversion rates $a^{ch/di}$, which are lower than bulk-size CAESs. However, these rates are variable during the scheduling horizon, and the average efficiency of 71.16 % is harvested for SCAES which means a^{ch} and a^{di} can be calculated as 0.8435 if the approximate assumption of $a^{ch} = a^{di}$ is considered. Hence, as opposed to large-scale CAES which have $a^{ch} = a^{di} = 0.9$, this value can be regarded as a reference for future research in DNs. In this regard, it is hopeful that small-size CAESs can reach an efficiency close to the large-scale CAESs with the advancement phase change materials in thermal storages.

7) Performance analysis over the life cycle

This subsection investigates and compares the performance of SCAES with other alternative ES technologies (such as the Li-ion battery and EVCS technologies) for the whole life cycle. Their performance is simulated over a one-year cycle and will be normalized and expanded to their life cycle considering the ES capital cost. In this regard, the yearly load demand of the grid is generated with the same approach adopted for daily operation. Profile of solar power generation and price of energy are based on the data provided by Australian Energy Market Operator for the year 2019 [49]. Thermal parameters of SCAES are considered to be as same as Scenario 4 for all days. The required data of battery storage units are provided in [51]. Comparison of DSO profit employing SCAES, battery bank, and EVCS for a one-year period is depicted in Fig. 12 (daily in *subplot a* and cumulative in *subplot b*).

Obviously, it can be seen that the daily profit of using battery bank is higher than other technologies due to its higher electric-to-electric efficiency. However, considering different capital costs and number of life cycles for ES technologies, a fair comparison can be accomplished by considering these parameters. Based on [4], the total capital cost for a 2 MWh, 500 kW battery bank is estimated at $2–2.8 million, while this cost is estimated to be $0.72–1.3 million for SCAES. For a similar capacity of EVCS with the given number of chargers in this paper, a capital cost of $1.1–1.6 million is estimated [37]. The highest capital costs are selected for the comparison task in the next step. The numbers of charging cycles over life time for the battery bank, SCAES, and EVCS in the distribution grid are approximately 20000, 10000, 5000, respectively. Considering one full charge-discharge cycle per day, Fig. 12 (c) shows the life span profit considering the total capital expenditure of the ES unit. The cost of operation and maintenance (O&M) is neglected in this case study for all the technologies; However, CAES has the lowest O&M cost followed by EVCS and battery bank. It can be seen that the battery bank can provide the highest saving during the first 5000 cycles while having the highest capital cost. Obviously, SCAES can provide much more profit in the long term due to its longest life cycle

IV. Conclusion

In this paper, the application of a utility-size SCAES as a potential ES technology for the participation of ADS in the wholesale power market is proposed. The thermal modeling of SCAES brings a new thermal-electrical conversation rate which is suitable for SCAES utilization at the distribution level. The effectiveness of SCAES is evaluated by comparing EVCS performance in different scenarios of the sole and joint operation. Based on five operation scenarios presented in this study, the following results are obtained:

- Compared with EVCS, SCAES can assist the DSO to reach higher profits in the sole operation scenario. In addition, considering the benefits of SCAES over EVCS in the sense of power loss reduction and voltage profile improvement, SCAES can be employed as a reliant storage unit for other objectives in DN operation as well.
- Utilization of SCAES besides the EVCS can be an appropriate option for DSO to suitably tackle the uncertainty of EVCS, or other similar storages, in the joint operation mode.
- Although the SCAES thermal/electrical conversion rate 0.85 is currently lower than the corresponding rate 0.95 of bulk-size CAESs, the result of this study demonstrates that it is still an applicable ES technology for ADSs operation.
- Generation insufficiency as well as uncertainties of the solar units and EVCS during starting and ending hours of the day are mitigated using SCAES.

References

[1] M. H. Imani, M. J. Ghadi, S. Ghavidel, and L. Li, "Demand response modeling in microgrid operation: a review and application for incentive-based and time-based programs," *Renewable and Sustainable Energy Reviews,* vol. 94, pp. 486-499, 2018.

[2] M. Faisal, M. A. Hannan, P. J. Ker, A. Hussain, M. B. Mansor, and F. Blaabjerg, "Review of energy storage system technologies in microgrid applications: Issues and challenges," *IEEE Access,* vol. 6, pp. 35143-35164, 2018.

[3] M. J. Ghadi, S. Ghavidel, A. Rajabi, A. Azizivahed, L. Li, and J. Zhang, "A review on economic and technical operation of active distribution systems," *Renewable and Sustainable Energy Reviews,* vol. 104, pp. 38-53, 2019.

[4] E. Barbour, D. Mignard, Y. Ding, and Y. Li, "Adiabatic compressed air energy storage with packed bed thermal energy storage," *Applied energy,* vol. 155, pp. 804-815, 2015.

[5] M. J. Tessier, M. C. Floros, L. Bouzidi, and S. S. Narine, "Exergy analysis of an adiabatic compressed air energy storage system using a cascade of phase change materials," *Energy,* vol. 106, pp. 528-534, 2016.

[6] S. Mei *et al.*, "Paving the way to smart micro energy grid: concepts, design principles, and engineering practices," *CSEE Journal of Power and Energy Systems,* vol. 3, no. 4, pp. 440-449, 2017.

[7] H. Lund, G. Salgi, B. Elmegaard, and A. N. Andersen, "Optimal operation strategies of compressed air energy storage (CAES) on electricity spot markets with fluctuating prices," *Applied thermal engineering,* vol. 29, no. 5-6, pp. 799-806, 2009.

[8] B. Cleary, A. Duffy, A. OConnor, M. Conlon, and V. Fthenakis, "Assessing the economic benefits of compressed air energy storage for mitigating wind curtailment," *IEEE Transactions on Sustainable Energy,* vol. 6, no. 3, pp. 1021-1028, 2015.

[9] J. Cheng, R. Li, F. Choobineh, Q. Hu, and S. Mei, "Dispatchable Generation of a Novel Compressed-Air Assisted Wind Turbine and its Operation Mechanism," *IEEE Transactions on Sustainable Energy,* 2018.

[10] S. Shafiee, H. Zareipour, A. M. Knight, N. Amjady, and B. Mohammadi-Ivatloo, "Risk-constrained bidding and offering strategy for a merchant compressed air energy storage plant," *IEEE Transactions on Power Systems,* vol. 32, no. 2, pp. 946-957, 2017.

[11] P. Denholm and R. Sioshansi, "The value of compressed air energy storage with wind in transmission-constrained electric power systems," *Energy Policy,* vol. 37, no. 8, pp. 3149-3158, 2009.

[12] H. S. de Boer, L. Grond, H. Moll, and R. Benders, "The application of power-to-gas, pumped hydro storage and compressed air energy storage in an electricity system at different wind power penetration levels," *Energy,* vol. 72, pp. 360-370, 2014.

[13] S. Shafiee, H. Zareipour, and A. Knight, "Considering thermodynamic characteristics of a CAES facility in self-scheduling in energy and reserve markets," *IEEE Transactions on Smart Grid,* 2016.

[14] A. H. Alami, "Experimental assessment of compressed air energy storage (CAES) system and buoyancy work energy storage (BWES) as cellular wind energy storage options," *Journal of Energy Storage,* vol. 1, pp. 38-43, 2015.

[15] G. Venkataramani and V. Ramalingam, "Performance analysis of a small capacity compressed air energy storage system for renewable energy generation using TRNSYS," *Journal of Renewable and Sustainable Energy,* vol. 9, no. 4, p. 044106, 2017.

[16] S. Wang, X. Zhang, L. Yang, Y. Zhou, and J. Wang, "Experimental study of compressed air energy storage system with thermal energy storage," *Energy,* vol. 103, pp. 182-191, 2016.

[17] J. Cheng and F. Choobineh, "Microgrid expansion through a compressed air assisted wind energy system," in *2016 IEEE Power & Energy Society Innovative Smart Grid Technologies Conference (ISGT)*, 2016, pp. 1-5: IEEE.

[18] C. Fang, L. Chen, Y. Zhang, C. Wang, and S. Mei, "Operation of low-carbon-emission microgrid considering wind power generation and compressed air energy storage," in *Proceedings of the 33rd Chinese Control Conference*, 2014, pp. 7472-7477: IEEE.

[19] A. Gheiratmand, E. Ayoubi, and M. Sarlak, "Optimal operation of micro-grid in presence of renewable resources and compressed air energy storage," in *2017 Conference on Electrical Power Distribution Networks Conference (EPDC)*, 2017, pp. 131-136: IEEE.

[20] J. Zhang *et al.*, "A bi-level program for the planning of an islanded microgrid including CAES," *IEEE Transactions on Industry Applications,* vol. 52, no. 4, pp. 2768-2777, 2016.

[21] R. Latha, S. Palanivel, and J. Kanakaraj, "Frequency control of microgrid based on compressed air energy storage system," *Distributed Generation & Alternative Energy Journal,* vol. 27, no. 4, pp. 8-19, 2012.

[22] H. Ibrahim, K. Belmokhtar, and M. Ghandour, "Investigation of usage of compressed air energy storage for power generation system improving-application in a microgrid integrating wind energy," *Energy Procedia,* vol. 73, pp. 305-316, 2015.

[23] P. Lombardi *et al.*, "An A□CAES pilot installation in the distribution system: A technical study for RES integration," *Energy Science & Engineering,* vol. 2, no. 3, pp. 116-127, 2014.

[24] H. Ibrahim, A. Bourji, M. Ghandour, and A. Merabet, "Optimization of compressed air storage's volume for a stand-alone wind-diesel hybrid system," in *2013 IEEE Electrical Power & Energy Conference*, 2013, pp. 1-7: IEEE.

[25] J. Cheng and F. Choobineh, "Microgrid expansion through a compressed air assisted wind energy system," in *Innovative Smart Grid Technologies Conference (ISGT), 2016 IEEE Power & Energy Society*, 2016, pp. 1-5: IEEE.

[26] M. Diekerhof, S. Hecker, and A. Monti, "Modeling and optimization of industrial compressed-air energy systems for Demand Response," in *Energy Conference (ENERGYCON), 2016 IEEE International*, 2016, pp. 1-6: IEEE.

[27] E. Jannelli, M. Minutillo, A. L. Lavadera, and G. Falcucci, "A small-scale CAES (compressed air energy storage) system for stand-alone renewable energy power plant for a radio base station: A sizing-design methodology," *Energy,* vol. 78, pp. 313-322, 2014.

[28] A. Setiawan, A. Priyadi, M. Pujiantara, and M. Purnomo, "Sizing compressed-air energy storage tanks for solar home systems," in *Computational Intelligence and Virtual Environments for Measurement Systems and Applications (CIVEMSA), 2015 IEEE International Conference on*, 2015, pp. 1-4: IEEE.

[29] L. Rui, C. Laijun, Y. Tiejiang, and L. Chunlai, "Optimal dispatch of zero-carbon-emission micro Energy Internet integrated with non-supplementary fired compressed air energy storage system," *Journal of Modern Power Systems and Clean Energy,* vol. 4, no. 4, pp. 566-580, 2016.

[30] S. Habib, M. Kamran, and U. Rashid, "Impact analysis of vehicle-to-grid technology and charging strategies of electric vehicles on distribution networks–a review," *Journal of Power Sources,* vol. 277, pp. 205-214, 2015.

[31] Z. Min, C. Qiuyu, X. Jiajia, Y. Weiwei, and N. Shu, "Study on influence of large-scale electric vehicle charging and discharging load on distribution system," in *2016 China International Conference on Electricity Distribution (CICED)*, 2016, pp. 1-4: IEEE.

[32] W. Su and K. Zhang, "Investigating the impact of plug-in electric vehicle charging on power distribution systems with the integrated modeling and simulation of transportation network," in *2014 IEEE transportation electrification conference and expo (Asia-Pacific), Beijing, China*, 2014, vol. 31.

[33] F. Jozi, K. Mazlumi, and H. Hosseini, "Charging and discharging coordination of electric vehicles in a parking lot considering the limitation of power exchange with the distribution system," in *2017 IEEE 4th International Conference on Knowledge-Based Engineering and Innovation (KBEI)*, 2017, pp. 0937-0941: IEEE.

[34] J. Hu, S. You, M. Lind, and J. Østergaard, "Coordinated charging of electric vehicles for congestion prevention in the distribution grid," *IEEE Transactions on Smart Grid,* vol. 5, no. 2, pp. 703-711, 2013.

[35] M. R. Sarker, H. Pandžić, and M. A. Ortega-Vazquez, "Optimal operation and services scheduling for an electric vehicle battery swapping station," *IEEE transactions on power systems,* vol. 30, no. 2, pp. 901-910, 2014.

[36] Y. Song, Y. Zheng, and D. J. Hill, "Optimal scheduling for ev charging stations in distribution networks: A convexified model," *IEEE Transactions on Power Systems,* vol. 32, no. 2, pp. 1574-1575, 2016.

[37] Z. Moghaddam, I. Ahmad, D. Habibi, and Q. V. Phung, "Smart charging strategy for electric vehicle charging stations," *IEEE Transactions on Transportation Electrification,* vol. 4, no. 1, pp. 76-88, 2017.

[38] Y. Zhang, P. You, and L. Cai, "Optimal charging scheduling by pricing for ev charging station with dual charging modes," *IEEE Transactions on Intelligent Transportation Systems,* 2018.

[39] M. Hosseini Imani, M. Jabbari Ghadi, S. Shamshirband, and M. Balas, "Impact evaluation of electric vehicle parking on solving security-constrained unit commitment problem," *Mathematical and Computational Applications,* vol. 23, no. 1, p. 13, 2018.

[40] M. H. Imani, K. Yousefpour, M. J. Ghadi, and M. T. Andani, "Simultaneous presence of wind farm and V2G in security constrained unit commitment problem considering uncertainty of wind generation," in *2018 IEEE Texas Power and Energy Conference (TPEC)*, 2018, pp. 1-6: IEEE.

[41] J. P. Coutier and E. Farber, "Two applications of a numerical approach of heat transfer process within rock beds," *Solar Energy,* vol. 29, no. 6, pp. 451-462, 1982.

[42] S. Ergun, "Fluid flow through packed columns," *Chem. Eng. Prog.,* vol. 48, pp. 89-94, 1952.

[43] M.-A. Rostami, A. Kavousi-Fard, and T. Niknam, "Expected cost minimization of smart grids with plug-in hybrid electric vehicles using optimal distribution feeder reconfiguration," *IEEE Transactions on Industrial Informatics,* vol. 11, no. 2, pp. 388-397, 2015.

[44] J.-H. Teng, "A direct approach for distribution system load flow solutions," *IEEE Transactions on power delivery,* vol. 18, no. 3, pp. 882-887, 2003.

[45] L. P. Fernandez, T. G. San Román, R. Cossent, C. M. Domingo, and P. Frias, "Assessment of the impact of plug-in electric vehicles on distribution networks," *network,* vol. 16, p. 21, 2011.

[46] M. Bakhshipour, M. J. Ghadi, and F. Namdari, "Swarm robotics search & rescue: A novel artificial intelligence-inspired optimization approach," *Applied Soft Computing,* vol. 57, pp. 708-726, 2017.

[47] K. Miettinen, M. M. Mäkelä, and J. Toivanen, "Numerical comparison of some penalty-based constraint handling techniques in genetic algorithms," *Journal of Global Optimization,* vol. 27, no. 4, pp. 427-446, 2003.

[48] M. Kashem, V. Ganapathy, G. Jasmon, and M. Buhari, "A novel method for loss minimization in distribution networks," in *DRPT2000. International Conference on Electric Utility Deregulation and Restructuring and Power Technologies. Proceedings (Cat. No. 00EX382)*, 2000, pp. 251-256: IEEE.

[49] A. Poullikkas, G. Kourtis, and I. Hadjipaschalis, "Parametric analysis for the installation of solar dish technologies in Mediterranean regions," *Renewable and Sustainable Energy Reviews,* vol. 14, no. 9, pp. 2772-2783, 2010.

[50] S. Rezaee, E. Farjah, and B. Khorramdel, "Probabilistic analysis of plug-in electric vehicles impact on electrical grid through homes and parking lots," *IEEE Transactions on Sustainable Energy,* vol. 4, no. 4, pp. 1024-1033, 2013.

[51] M. J. Ghadi, A. Rajabi, S. Ghavidel, A. Azizivahed, L. Li, and J. Zhang, "From active distribution systems to decentralized microgrids: A review on regulations and planning approaches based on operational factors," *Applied Energy,* vol. 253, p. 113543, 2019.

Mojtaba Jabbari Ghadi is pursuing the Ph.D. degree in electrical engineering at the University of Technology Sydney, Sydney, Australia.

Ali Azizivahed is pursuing the Ph.D. degree in electrical engineering at the University of Technology Sydney, Sydney, Australia.

Amin Rajabi is currently pursuing the Ph.D. degree in electrical engineering at the University of Technology Sydney, Sydney, Australia.

Sahand Ghavidel is currently pursuing the Ph.D. degree in electrical engineering at the University of Technology Sydney, Sydney, Australia.

Li Li is currently an Associate Professor at the University of Technology Sydney, Sydney, Australia.

Jiangfeng Zhang is currently an Associate Professor at the University of Technology Sydney, Sydney, Australia.

Miadreza Shafie-khah (M'13-SM'17) is currently an Assistant Professor at the University of Vaasa, Vaasa, Finland.

João P. S. Catalão (M'04-SM'12) is currently a Professor at the Faculty of Engineering of the University of Porto (FEUP), Porto, Portugal, and Research Coordinator at INESC TEC.